Performance of an integrated solar absorption cooling system in a sub-tropical region

J. Darkwa* **and S. Fraser**

Centre for Sustainable Energy Technologies (CSET), University of Nottingham Ningbo, 199 Taikang East Road, Ningbo 315100, China

Abstract

Evaluation of an integrated solar absorption cooling system located in a sub-tropical region has been carried out. Analysis of the results revealed an operational efficiency of 61% for the solar collectors at a mean differential temperature (ΔT) of 51°C when compared with the manufacturer's rating of 70% at 60°C. The absorption chiller did, however, perform quite satisfactorily and achieved a coefficient of performance of 0.69 when compared with the manufacturer's rating of 0.7. There is however the need for the hot water supply system to be optimized as well as provision for supplementary heat source in order to maintain the appropriate operating temperature during low solar radiation levels.

Keywords: solar air-conditioning system; absorption chiller; collector efficiency; COP

*Corresponding author: jo.darkwa@nottingham.edu.cn

Received 7 December 2011; revised 10 February 2012; accepted 16 February 2012

1 INTRODUCTION

According to the World Business Council for Sustainable Development (WBCSD), buildings account for ~40% of final global energy consumption and carbon dioxide (CO_2) emissions (http://www.environmentalleader.com/2009/04/27/building-sector-needs-to-reduce-energy-use-60-by-2050/). It is also estimated that 85% of a building's gas emissions is caused by heating, cooling and lighting activities and that commercial buildings produce approximately one-third of energy-related CO_2 emissions worldwide [1]. In response to these findings, the International Energy Agency (IEA) has made some recommendations such as changes to building shells, application of heat pumps, solar heating/cooling and the use of renewables as means of reducing energy consumption and emissions levels [2]. Recent studies by Cullen *et al.* [3] have further proposed other measures that could save ~70% of global energy demand in buildings.

These measures are however likely to make impact if they could be promoted and implemented on large scale in some of the high energy-consuming countries such as China. For instance, energy usage in Chinese buildings currently accounts for ~30–36% of the country's total energy consumption and CO_2 emissions [4, 5]. The bulk of the energy consumption takes place in large public and government office buildings which consume ~10 times more energy than residential buildings (http://www.nbast.org.cn/1120/tools/institute/advice_read.php?id=13). Within these sectors, space heating, cooling and lighting account for the largest proportion of the energy usage [6]. According to Wang *et al.* [7], over two-thirds of China's land area receives ~6000 MJ/m^2/year of solar energy. If this resource could be well utilized for cooling the buildings, it could go a long way towards the reduction in final energy consumption and emissions levels. It appears that China has already taken the lead in exploiting this vast resource, since it currently has ~39% more installed capacity of active solar thermal systems than the rest of the world combined [8]. The overall performances of some of these systems have been evaluated and reported as satisfactory. For instance, Zhai *et al.* [9] evaluated one of the installations located in Shanghai and found that it is capable of providing 70% of the total yearly cooling load. Qu *et al.* [10] assessed the performance of another solar thermal cooling system and achieved ~50% cooling capacity.

Rosiek and Batlles [11] evaluated the performance of a solar-assisted 70 kW single-effect LiBr–Water chiller located in Spain and reported a maximum coefficient of performance (COP) of 0.6. Pongtornkulpanich *et al.* [12] investigated the performance of a single-effect LiBr–H_2O absorption chiller in Thailand. The system was driven by arrays of evacuated solar tubes but also had an integrated liquefied petroleum gas fired boiler to boost up heat source when there was insufficient irradiation. The system was reported to be capable of providing ~81% of the yearly cooling load. Ali *et al.* [13] assessed the performance of a 35 kW solar absorption cooling plant and

International Journal of Low-Carbon Technologies 2012, 7, 199–207

doi:10.1093/ijlct/cts024 Advance Access Publication 6 April 2012

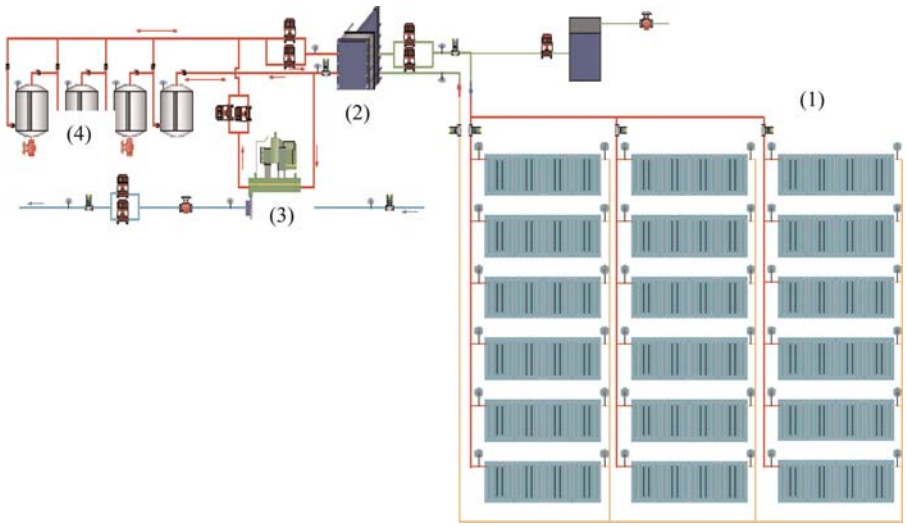

Figure 1. *Schematic view of the solar air-conditioning system.*

reported maximum collectors' field efficiency of 49.2% and a COP of 0.81. Other researchers [14–16] have also reported similar promising results.

Despite these encouraging feedbacks, there are other operational limitations and integration issues which appear to restrict the growth of the solar thermal systems in comparison with conventional cooling systems. For example, double-effect solar absorption cooling systems have twice the COP as much as single-effect types but require far higher operating temperatures which tend to result in higher energy losses. In terms of appropriate solar thermal collector, it is not a case of one size fits all. There is no 'best' collector for driving solar absorption systems as there are a range of individual factors that must all be taken into account on a case-by-case basis, in particular, the local climate, the collector output temperature, the installation angle and efficiency [17].

This study is therefore intended to evaluate the performance of a typical integrated solar absorption system located in a subtropical region in China, in order to highlight any operational or technical barriers affecting large-scale application.

2 SYSTEM DESCRIPTION

2.1 General

Figure 1 shows a schematic arrangement of the integrated solar cooling system as installed in the Centre for Sustainable Energy Technologies (CSET) building at the University of Nottingham, Ningbo, China. It consists of an array of evacuated solar collectors (1), set of flat-plate heat exchangers (2), an absorption water chiller (3) and four pieces of hot water storage tanks (4).

2.2 Evacuated solar collector tubes

Figure 2 shows the array of evacuated U-tube solar collectors as installed on site (Solar Energy Co. Ltd., China). In order to make the most of any available radiation, the collectors were installed to face directly south at an angle of 25° with a net absorption area of 220 m^2. According to the manufacturer's rating, the system should be able to operate at 84% efficiency when the difference between the inlet fluid and external air $(\Delta T) = 0°C$ and at 70% efficiency when $(\Delta T) = 60°C$. The system is fitted with an expansion tank to negate the effects of any thermal expansion that may occur. The piping is insulated to limit the amount of energy losses during heat transfer between the collectors and the hot water storage tanks.

Figure 2. *Array of solar collectors.*

2.2.1 *Solar collectors tilt angle*

The collector array field was oversized by using the mean solar radiation value for the month of July (being the hottest month of the year), instead of the maximum summer solar radiation. This was to ensure the availability of adequate heat supply in

the event of low solar radiation level. For the benefit of obtaining the best tilt angle for the year, initial simulation exercise was carried out for both winter and summer periods. The calculation was performed by means of the relevant routines of EnergyPlus applied to the Test Reference Year for the city of Hangzhou (Lat. 30°N), which is the closest city to Ningbo in the EnergyPlus database. Figure 3 shows for different tilt angles (from 15° to 55°) and the corresponding maximum energy collectable per unit area.

The results show that different tilt angles are not so relevant, and, even more so, the energy collected during the summer period (the most important in this case) is higher for lower tilt angle. A tilt angle of 25° was however considered to be the optimum for the installation.

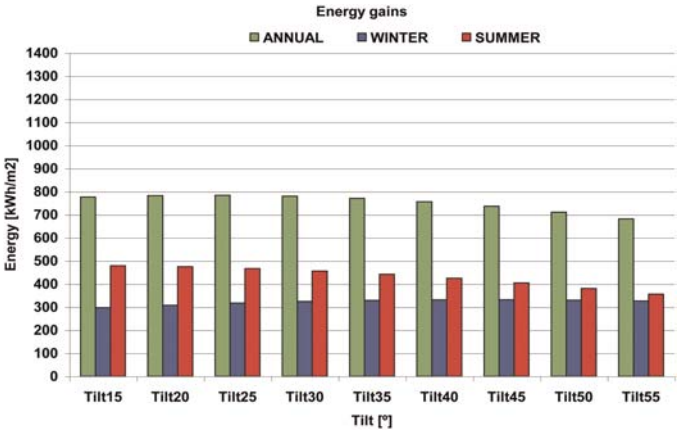

Figure 3. *Yearly energy gains.*

2.3 Heat exchanger

A flat-plate heat exchanger as shown in Figure 4 was installed with the following specification:

Water to water plates heat exchanger at 160 kW
Primary: fluid = glycol/water solution (30% glycol + 70% water); inlet/outlet temperature = 100/90°C; inlet/outlet diameter = 70 mm; water flow rate = 15 m^3/h.
Secondary: fluid = water; inlet/outlet temperature = 88/98°C; inlet/outlet diameter = 50 mm; water flow rate = 15 m^3/h.

Figure 4. *Flat-plate heat exchanger.*

2.4 Water storage tanks

The water tanks as shown in Figure 5 have a total capacity of 16 000 l (4000 l/tank) and have been placed in series in order to maintain controlled temperature stratification. Thermally stratified storage tanks are effective means of storing intermittent source of energy and for situations where time lag exists between the production and the demand.

2.5 Absorption water chiller

Figure 6 shows a schematic view of the hot water-powered absorption chiller, type SYBCTDH115. The system uses LiBr–H_2O solution as the working fluid to produce chilled water at 7°C for the air handling units. It has a cooling capacity of 55 kW with an inlet/outlet hot water temperature of 90/80°C and a COP of 0.7.

3 METEOROLOGICAL AND OPERATIONAL DATA

3.1 Methodology

The global solar radiation and meteorological data were collected over the summer period. Due to faulty operational sensors, the data for the month of August were selected instead of July which is the hottest month of the year. Calibrated operational data from 12 noon to 4 p.m. for a period of 7 days

Figure 5. *Hot water storage tanks.*

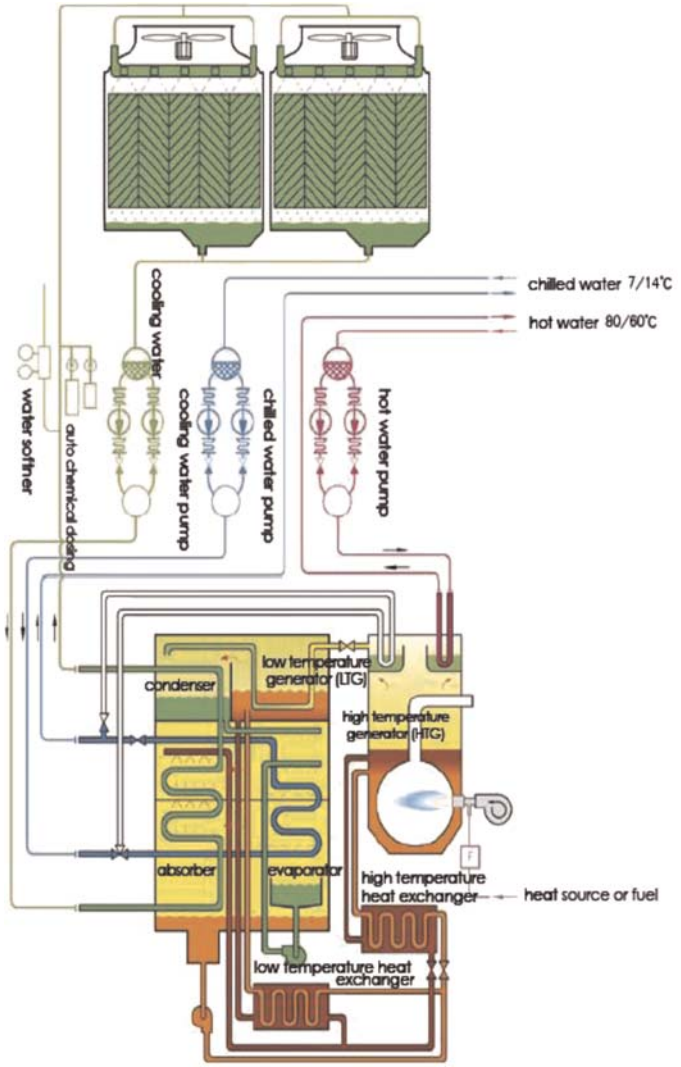

Figure 6. *Absorption water chiller (http://www.archiexpo.com/prod/broad-air-conditioning-europe-sas/absorption-chillers-58929-149764.html).*

Table 1. *Equipment specifications.*

Equipment	Type	Measured parameters	Resolution	Accuracy
Columbia Orion	LX200	Wind speed (m/s)	1 m/s	±3% (0–35 m/s)
Fixed-Mount		Air temperature (°C)	0.1°C	±0.3°C at +20°C
Weather Station		Relative humidity (%)	1%	±3%
		Dew point (°C)	0.1°C	±0.3°C at +20°C
		Rain fall (mm)	0.254 mm	±5%
Hukseflux solar radiation sensor		Global solar radiation ($W/m^{2)}$	305–2800 nm	15 $\mu V/W/m^2$

(9th–10th, 16th, 19th and 23rd–26th) in August 2010 were therefore used for the evaluation exercise. Table 1 shows the list of equipment that was used for measuring the data.

3.2 Weather

3.2.1 *Theoretical solar radiation*

A simplified solar radiation model based on the latitude, the day of the year and the tilt of the plane was considered. In this manner, it was possible to estimate the radiation available to the solar collectors for the month of August by using the following general equations [18]:

Declination:

$$\delta = 23.45 \sin\left[\frac{360\,(284+n)}{365}\right] \tag{1}$$

where n is the day number.

Sunset angle (ω_s):

$$\cos\omega_s = -\tan\Phi\tan\delta \tag{2}$$

where Φ = site latitude.

Daylight hours:

$$N = \frac{2\cos^{-1}(-\tan\Phi\tan\delta)}{15\cos\omega_s} \tag{3}$$

Solar time (sunrise and sunset time, respectively)

$$t = 12 \pm \frac{N}{2} \tag{4}$$

Solar hour angle: (ω)

$$\omega = 15(12-t) \tag{5}$$

Incidence angle, theta (θ):

$$\begin{aligned}\cos\theta = {} & \sin\delta\sin\Phi\cos\beta - \sin\delta\cos\Phi\sin\beta\cos\gamma \\ & + \cos\delta\cos\Phi\cos\beta\cos\omega \\ & + \cos\delta\sin\Phi\sin\beta\cos\gamma\cos\omega \\ & + \cos\delta\sin\beta\sin\gamma\sin\omega\end{aligned} \tag{6}$$

where β is the tilt angle and γ the surface azimuth angle.

Zenith angle: (z)

$$\cos\theta_z = \sin\delta\ \sin\Phi\ +\ \cos\delta\ \cos\Phi\ \cos\omega \tag{7}$$

The proportion of beam radiation on a tilted to a horizontal plane:

$$R_b = \frac{\cos\theta}{\cos\theta z} \tag{8}$$

Extraterrestrial solar irradiance:

$$G_o = G_{sc}\left[1 + 0.033\cos\left(\frac{360n}{365}\right)\right]\cos\theta_Z \tag{9}$$

where G_{sc} is the solar constant.

Hourly energy from irradiance:

$$H_o = G_o \times \text{Time} = G_o \times 1\,\text{h}\,(\text{Wh/m}^2) \quad (10)$$

Solar radiation at the ground level—horizontal surface:

$$H = k_t H_o \quad (11)$$

where $k_t$is the clear sky index

Diffuse radiation (when $\omega_s \leq 81.4$ and $0.3 \leq k_t \leq 0.8$)

$$\frac{H_d}{H} = 1.391 - 3.56\,k_t + 4.189\,k_t^2 - 2.137\,k_t^3 \quad (12)$$

Diffuse radiation (when $\omega_s > 81.4^0$ and $0.3 \leq k_t \leq 0.8$)

$$\frac{H_d}{H} = 1.311 - 3.022k_t + 3.427k_t^2 - 1.821k_t^3 \quad (13)$$

Beam radiation:

$$H_b = H - H_d \quad (14)$$

Radiation on the tilted plane:

$$H_t = H_b R_b + H_d\left[\frac{1+\cos\beta}{2}\right] + H\rho_g\left[\frac{1-\cos\beta}{2}\right] \quad (15)$$

where ρ_g is the ground reflectivity.

Using the above equations and the data below, the profile of the mean daily theoretical radiation on the solar collectors was obtained as shown in Figure 7.

Data:

- The solar collectors face due south (Azimuth = 0) and have a tilt angle (β) of 25°.
- G_{sc}= 1367 W/m^2
- Given that the collectors are located on a grassy lawn, the ground reflectivity (ρ_g) was set at 0.2 [19].
- Clear sky index (k_t) was assumed to be 0.5 based on the general weather condition at that time of the year in Ningbo.

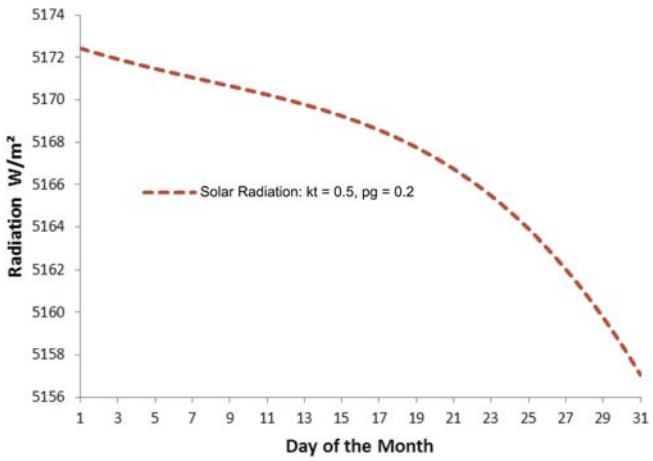

Figure 7. *Theoretical total daily solar radiation for August.*

3.2.2 *Measured solar radiation*

Figure 8 shows the instantaneous measured solar radiation levels for the selected dates which appear to fluctuate slightly more from each day to the next. It is however clear that the radiation levels reached their peak between 12:50 and 14:30 for most of the days. The maximum solar radiation of 944 W/m^2 was recorded on 19 August at ~12:50.

Figure 9 compares the mean hourly theoretical and the measured radiation profiles for the selected dates. As expected, the actual radiation levels did fluctuate much more wildly in comparison with the theoretical model which does not take into account the haze and cloud levels on a day-to-day basis but instead uses a fixed clear sky index as a general estimate. Nevertheless, the two profiles followed similar trends and achieved identical values at 16:00.

3.2.3 *Measured ambient temperature*

Figure 10 represents the profiles for the instantaneous ambient temperatures over the selected dates. The maximum mean

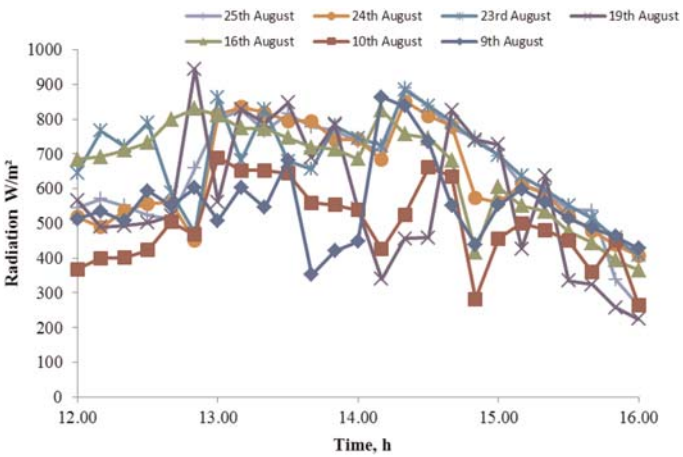

Figure 8. *Instantaneous solar radiation profiles.*

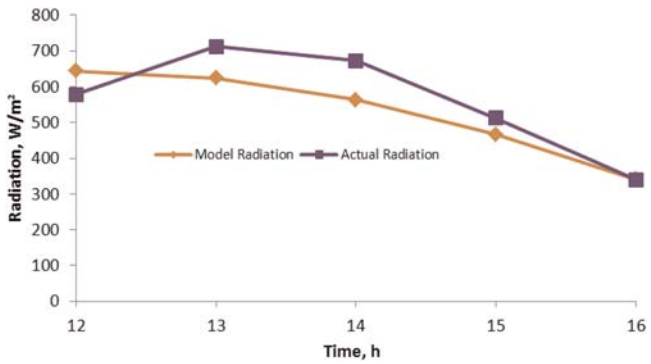

Figure 9. *Mean hourly radiation profiles for selected dates.*

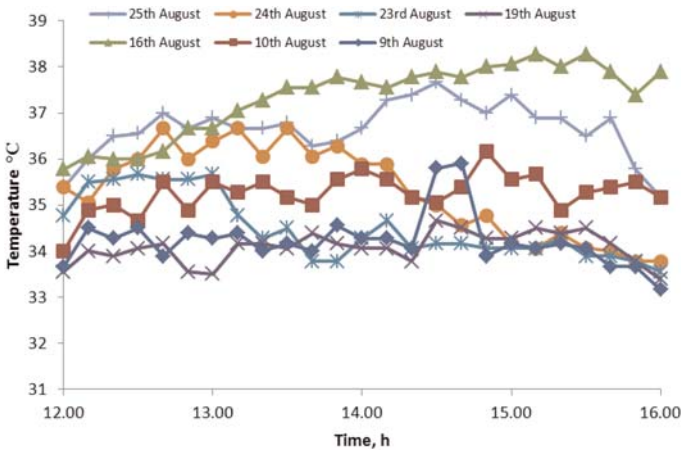

Figure 10. *Instantaneous ambient temperature profiles.*

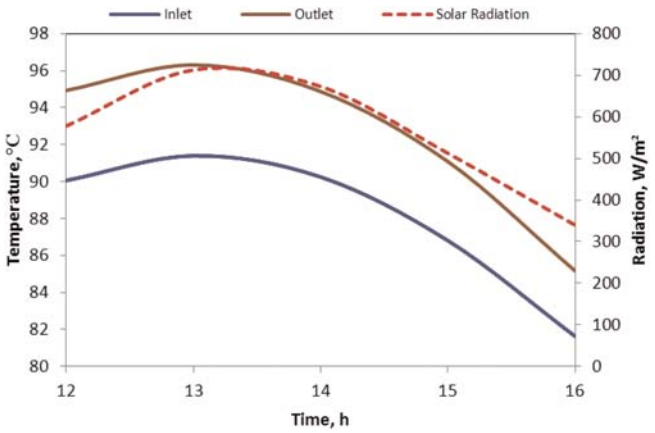

Figure 11. *Average hourly temperatures and radiation levels.*

temperature was recorded on 16 August as 37.2°C, whereas the average for the other days was between 30 and 31.5°C

3.3 Operational data

The operational data from the evacuated tube collectors and the absorption chiller unit were collected at every 10 min interval using a Honeywell Building Management System. The data for the evacuated tube collectors consisted of the inlet and outlet temperatures of the circulating fluid, whereas the inlet and outlet temperatures of the generator and evaporator were recorded for the absorption unit.

3.3.1 *Solar collector*

The average hourly inlet and outlet temperatures for the solar collectors are presented in Figure 11. It can be seen that the peak inlet/outlet temperatures of 91.4°C/96.3°C occurred between 13:00 and 14:00 on each day. The differential temperature between the two fluids was somehow almost constant between 12:00 and 14:00 until it steadily declined in accordance with the fading radiation levels.

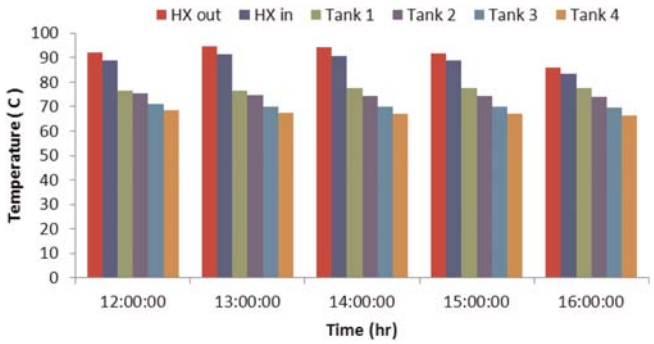

Figure 12. *Mean hourly temperature profiles for selected dates.*

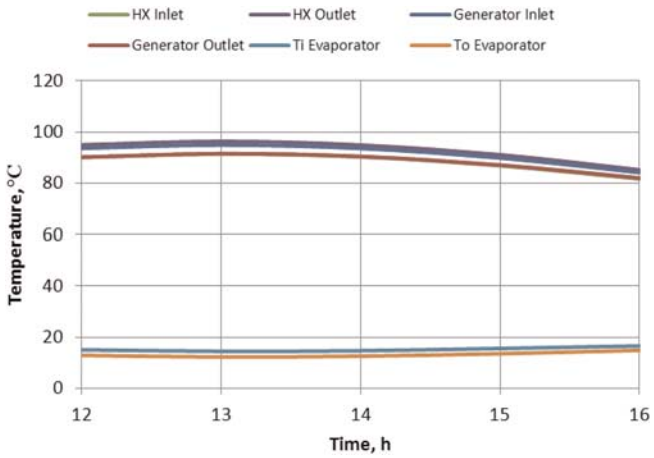

Figure 13. *Temperature profiles in the evaporator, generator and collector.*

3.3.2 *Hot water storage tanks*

Figure 12 shows the mean hourly water temperature profiles inside the storage tanks and the water flowing in and out of the tanks (heat exchanger). The graph shows that Tank 1 recorded the maximum temperature of 77.7°C at 3 p.m. with Tank 4 recording the lowest temperature of 66.3°C at 4 p.m. These values support the installation arrangement in Figure 5 where Tank 1 is the first to be supplied by the heat exchanger (HX) before the rest of the tanks. The arrangement did also control temperature stratification as planned and therefore did ensure fairly and steady storage temperature distribution in the tanks.

3.3.3 *Absorption chiller*

The mean hourly temperatures were ascertained for both the evaporator and the generator during the period of operation. As shown in Figure 13, most of the cooling by the evaporator occurred between 13:00 and 14:00 with an average cooling temperature of 12.2°C. Obviously, the peak performance of the generator, evaporator and the HX occurred within the same period. As a result, the average inlet temperature of the HX and the outlet temperature of the absorption generator were very similar. The same is true of the generator inlet and

collector outlet temperatures with the former being slightly less than the latter due to some heat loss at the heat exchanger end.

4 PERFORMANCE OF SYSTEMS

4.1 Collector efficiency

The instantaneous theoretical and practical efficiencies for the solar collector were calculated using the following equation:

$$\eta = \frac{m \times c_p \times (T_i - T_o)}{I \times A} \tag{16}$$

where m is the mass fluid flow rate (4.2 kg/s), c_p the specific heat (4.2 kJ/kg/K), A the net solar collector area (220 m^2), T_i the inlet fluid temperature, T_o the outlet fluid temperature, I the solar radiation (theoretical or measured).

For the purpose of comparison, the manufacturer's efficiency based on given loss coefficients [20] was also calculated using Equation (17).

$$\eta_{\Delta t} = \eta_0 - \vartheta_{1*}\Delta t - \vartheta_{2*} I \times \Delta t^2 \tag{17}$$

$$\eta_{\Delta t} = 0.717 - 1.52 \times \frac{T_m - T_a}{I} - 0.0085 \times \left[\frac{T_m - T_a}{I}\right]^2 \tag{18}$$

where η_0, ϑ_1 and ϑ_2 are manufacturer's loss coefficients, T_m, T_m the mean temperature of the circulating fluid (inlet and outlet temperature) and T_a the ambient temperature.

The average theoretical and the practical efficiencies with respect to the corresponding solar radiation levels are presented in Figure 14. In most cases, the practical and theoretical efficiency curves differed quite significantly throughout the course of the day as they were dictated by the solar radiation levels. The efficiencies dropped quite significantly when the radiation levels peaked between 1:30 p.m. and 2:30 p.m. before ascending again in the late afternoon as the amount of radiation gradually faded. The manufacturer's efficiency curve however loosely followed the solar radiation levels.

The mean instantaneous collector efficiencies were also calculated and presented in Figures 15 and 16. Analysis of the results gives an operational efficiency of 61% when compared with 56% for the manufacturer's efficiency. In reality, the measured efficiency would be slightly lower since the calculations do not take into account the heat loss coefficients and removal factor. Further analysis reviews that the solar collectors did underperform when compared with the manufacturer's rating, which states that the efficiency at $\Delta T = 0^\circ C$, should be 84% and at $\Delta T = 60^\circ C$ should be 70% (where ΔT is the difference between the inlet fluid and ambient air temperature).

In all recorded instances, ΔT was found to be lower than 60°C as the mean value attained was 51.3°C. This level of underperformance could be attributed to a number of factors. For instance, the manufacturer's efficiency rating and loss coefficients were likely based on a different optimum tilt angle. Normally, solar collectors are installed at an angle equal to the latitude of the site. However, depending on whether the primary load is experienced during summer or winter, the angle can be adjusted by $\pm 15^\circ$ to account for the varying declination of the Sun throughout the year. Therefore, given the time of the year that the data were collected, it is possible that a lower tilt angle could have led to a slightly better system performance as demonstrated in Figure 3 with different tilt angles.

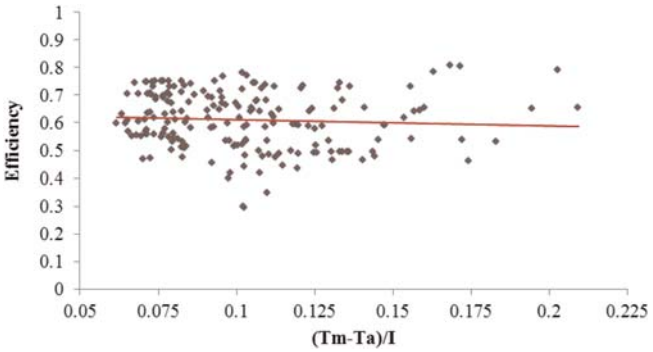

Figure 15. *Instantaneous collector field efficiency: practical.*

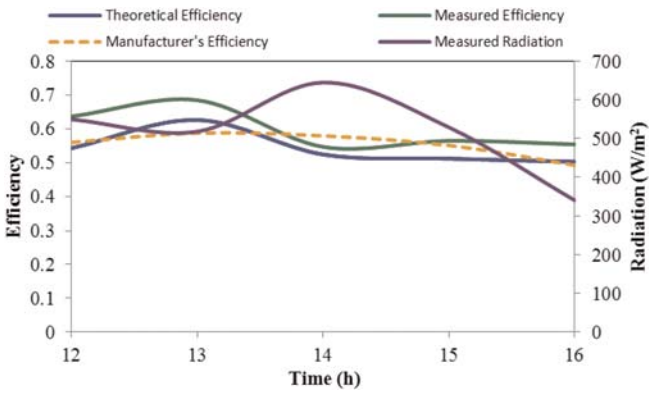

Figure 14. *Mean hourly efficiencies and radiation profiles.*

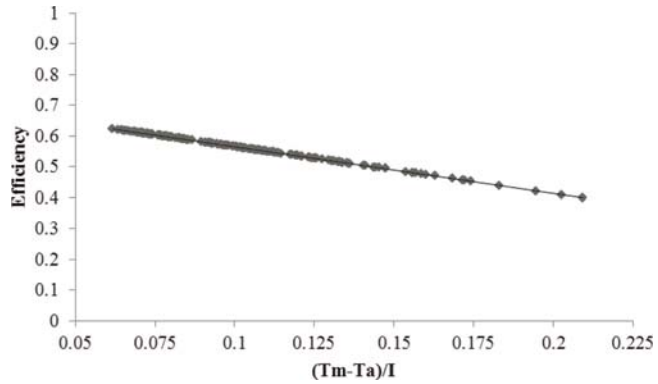

Figure 16. *Instantaneous collector field efficiency: manufacturer.*

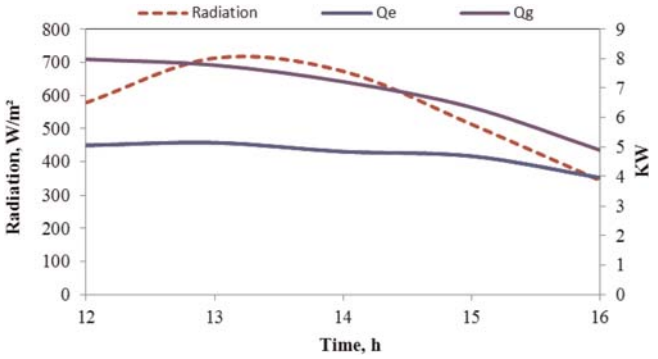

Figure 17. *Mean hourly profiles of* Q_e, Q_g *and radiation.*

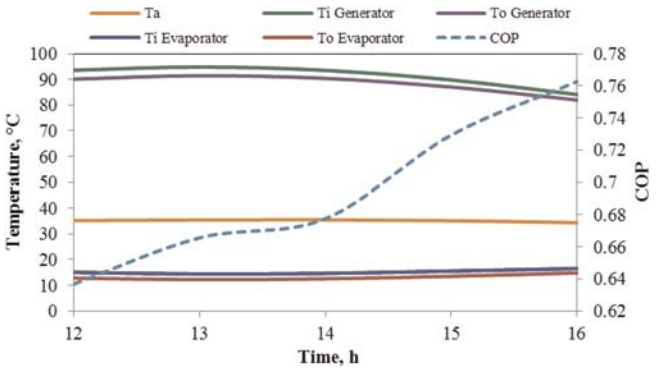

Figure 18. *Mean hourly chiller performance.*

4.2 COP of the chiller

The COP of the chiller was calculated based on the operational data and Equations (18–20).

$$\mathrm{COP} = \frac{Q_e}{Q_g} \tag{19}$$

Evaporator cooling capacity

$$Q_e = m_{fe}\Delta T_e \tag{20}$$

Heat input to the generator

$$Q_g = m_{fg}\Delta T_g \tag{21}$$

where m_{fe} and m_{fg} are the water flow rates (kg/s) in the evaporator and the generator, respectively, ΔT_e and ΔT_g are the temperature differences in respective fluid flows.

It can be seen in Figure 17 that Q_e remained far more stable than Q_g which was prone to fluctuations from the radiation levels. In general, the gap between the two profiles was greatest from 12:00 and 1:00 p.m. and then slowly decreased in accordance with the fading radiation levels. The COP however steadily increased from 0.64 at noon to 0.76 by 16:00 and was largely accredited to the control strategy of the chiller and the stability of the evaporator inlet and outlet temperatures as shown in Figure 18. The mean COP of the absorption chiller was obtained as 0.69, which is almost identical to the manufacturer's rating of 0.7.

5 CONCLUSION

The aim of this study was to assess the performance of a typical integrated solar hot water absorption cooling system located in a sub-tropical region. For the benefit of comparison, the theoretical, practical and the manufacturer's efficiencies were established for the evacuated tube collectors. In the case of the absorption chiller, the COP was determined based on the measured heat input and the cooling capacity data. The specific findings are summarized below.

- The theoretical collector efficiency was obtained as 69%.
- The practical or operational collector efficiency was obtained as 61% at a mean differential temperature (ΔT) of 51°C.
- The manufacturer's collector efficiency was obtained as 56%.
- The absorption chiller achieved a COP equivalent to 0.69.

There was however a slight deviation of the practical collector efficiency when compared with the manufacturer's rating which requires the efficiency to be 70% for a ΔT of 60°C. Although the theoretical efficiency meets this rating, it does not take into account the heat loss coefficient and removal factor of the evacuated tubes. On the other hand, the absorption chiller performed quite satisfactorily with a COP of 0.69 when compared with the manufacturer's rating of 0.7. The installation strategy adopted for controlling temperature stratification appears to have achieved its objective and ensured a fairly temperature distribution profiles in the tanks. The integrated solar absorption system has therefore proved its potential as a viable cooling technology for buildings. There is however the need for the hot water supply system to be optimized as well as provision for supplementary heat source such as gas- or biomass-fired system in order to provide an appropriate operating temperature during low solar radiation levels.

REFERENCES

[1] *Energy Technology Perspectives 2008*. International Energy Agency, 2008.
[2] IEA. *Technology Roadmaps—Energy-Efficient Buildings: Heating and Cooling Equipment*. 2011.
[3] Cullen JM, Allwood M, Borgstein EH. Reducing energy demand: what are the practical limits? *Environ Sci Technol* 2011;**45**:1711–8.
[4] Li B, Yao R. Urbanisation and its impact on building energy consumption and efficiency in China. *Renew Energy* 2009;**34**:1994–8.
[5] Dhakal S. Urban energy use and carbon emissions from cities in China and policy implications. *Energy Policy* 2009;**37**:4208–19.
[6] China Urban Research Committee. *Chinese, Construction Industrial Publish House*, 2008. ISBN 978-7-112-09925-2.

[7] Wang RZ, Zhai XQ. A review for absorption and adsorption solar cooling systems in China. *Renew Sustain Energy Rev* 2009;**13**:1523–31.
[8] Weiss W, Mauthner F. *Solar Heat Worldwide: Market and Contribution to the Energy Supply 2008*. IEA Solar Heating and Cooling Programme, 2010.
[9] Zhai XQ, Wang RZ, Wu JY, *et al*. Solar integrated energy system for a green building. *Energy Build* 2007;**39**:985–93.
[10] Qu M, Yin H, Archer DH. A solar thermal cooling and heating system for a building: experimental and model based performance analysis and design. *Sol Energy* 2010;**84**:166–82.
[11] Rosiek S, Batlles FJ. Integration of the solar thermal energy in the construction: analysis of the solar-assisted air conditioning system installed in the CIESOL building. *Renew Energy* 2009;**34**:1423–31.
[12] Pongtornkulpanich A, Thepa S, Amornkitbamrun M, *et al*. Experience with fully operational solar-driven 10-ton LiBr/H_2O single-effect absorption cooling system in Thailand. *Renew Energy* 2008;**33**:943–9.
[13] Ali AHH, Noeres P, Pollerberg C. Performance assessment of an integrated free cooling and solar powered single-effect lithium bromide-water absorption chiller. *Sol Energy* 2008;**82**:1021–30.
[14] Bermejo P, Pino FJ, Rosa F. Solar absorption cooling plant in Seville. *Sol Energy,* 2010;**84**:1503–12.
[15] Assilzadeh F, Kalogirou SA, Ali Y, *et al*. Simulation and optimization of a LiBr solar absorption cooling system with evacuated tube collectors. *Renew Energy,* 2005;**30**:1143–59.
[16] Monne C, Alonso S, Palacin F, *et al*. *Int J Refriger* 2011;**34**:518–26.
[17] IEA. On-going research relevant for solar assisted air conditioning systems. *Technical Report Task 25: Solar Assisted Air-Conditioning of Buildings*. International Energy Agency, 2002.
[18] Duffie JA, Beckman WA. *Solar Engineering of Thermal Processes*. Wiley, 1991.
[19] Quaschning V. *Understanding Renewable Energy Systems*. Earthscan, 2005.
[20] Jiangsu Sunrain Solar Energy Co., Ltd. Data catalogue.